Title: Atmosphere-Land Coupling and the Predictability of North American Drought

Institution: University of Miami, Rosenstiel School of Marine and Atmospheric Science

Investigators: Benjamin Kirtman (PI), Brian Mapes (Co-PI) and Chidong Zhang (Co-PI).

Final Report: 1 August 2010 – 31 July 2014

NA10OAR4310164

1. Introduction

The proposed research is based on the hypothesis that the predictability of persistent large-scale drought is due the competition of among three processes:

(i) The nature of local coupled atmosphere-land feedbacks (i.e., strength, growth rate, saturation)

(ii) The predictability limiting affects of atmospheric noise or stochastic forcing

(iii) The remote forcing from low frequency global SST variability (e.g., AMO, PDO, NPO…).

We propose to test this hypothesis through a series of modeling experiments that isolate the relative importance of coupled atmosphere-land feedbacks vs. atmospheric stochastic forcing vs. remote SST forcing. These experiments include using the novel interactive ensemble coupling strategy (Kirtman and Shukla 2002) previously used to isolate coupled ocean-atmosphere feedbacks vs. atmospheric stochastic forcing applied to the problem atmosphere-land interactions and novel numerical experiments were SSTA in specific regions are prescribed within the context of the coupled model. Part of our modeling strategy builds on the success of the US Clivar drought WG (http://www.usclivar.org/Organization/drought-wg.html) and the international Global Land-Atmosphere Coupling Experiment (GLACE) by explicitly leveraging their experimental protocol. We have chosen to focus on the question of North American drought because of its societal importance to US interests; however, the approach is equally applicable to terrestrial hydro-climate predictability on multiple space and time scales throughout the globe.

To understand the predictability of North American drought we adopt the framework that was first developed to understand *atmosphere-ocean* feedbacks and apply it to *atmosphere-land* interactions. To understand how we envision that adoption we note that Hasslemann (1976) hypothesized that mid-latitude ocean variability could be understood as the zero-dimensional (0-D) red-noise thermodynamic uncoupled ocean mixed-layer response to white noise atmospheric stochastic forcing. More recently, Barsugli and Battisti (1998) generalized the Hasslemann (1976) hypothesis to include coupled atmosphere-ocean feedbacks, which further redden the response. Wu and Kirtman (2007) showed how the Barsugli and Battisti (1998) model could be applied to the tropics and used to understand air-sea feedbacks in coupled models (see also Wu et al. 2007). Indeed, there is extensive literature looking at the nature of air-sea feedbacks and how this is modified by ocean dynamics that is too large to adequately review here.

Results presented here highlight: (a) the impact of atmosphere-land initialization in seasonal prediction experiments; (b) the predictability of southeast US drought from a multi-model prediction perspective and (c) modifications to the interactive ensemble coupling strategy that are specifically designed to diagnose atmosphere-land feedbacks.

2. Results and Accomplishments

a. Predictability of southeast US Rainfall

Infanti and Kirtman (2014a) chose to focus on the 2006–07 dry period in order to examine the skill of the NMME system in hindcasting individual events. This period involved below-normal rainfall (phase 1), followed by a brief reprieve (phase 2) before a stronger period of below-normal rainfall (phase 3), thus highlighting the need for seasonality within an event. This period was also studied by Seager et al. (2009), who found that the dry period was not accurately represented by a Global Ocean Global Atmosphere (GOGA) model using 6-month averages,

and the model failed to create a continuous drought. We believe that it is important to examine the seasonality of this drought as it highlights some of the prediction challenges.

We have plotted southeastern U.S. precipitation plumes for the 2006–07 dry period in Figs. 1a (February starts) and 8b (September starts). Figure 1a shows hindcasts initialized in (left to right) February 2005, 2006, and 2007, with lead time increasing along the *x* axis. Figure 1b shows hindcasts initialized in (left to right) September 2005, 2006, and 2007. The blue line indicates the NMME ensemble mean anomaly, the red line indicates observed precipitation anomaly, and the gray lines indicate individual ensemble member anomalies. All anomalies are standardized (divided by standard deviation). Blue shading refers to phases 1, 2, and 3 of this drought. Anomalies are 3-month running means. It becomes apparent that observations show a brief below-normal period in early 2006 (phase 1), followed by a slight reprieve in mid-2006 (phase 2), then a stronger below-normal period in early 2007 (phase 3).

The plumes in Figs. 1a and 1b show constant range of ensemble members throughout all lead times and during the two hindcast initialization months; thus, the uncertainty at all lead times remains constant. We find good agreement between ensemble mean and observations during the first phase of the dry period when considering February starts (Fig. 1a, middle), and the ensemble mean stays neutral or weakly dry through phases 2 and 3. When looking at September hindcast initialization (Fig. 1b), there is less agreement between observations and the ensemble mean overall. September hindcast initialization shows some drying during phase 1 of the drought (Fig. 1b, left) and captures the precipitation increase during phase 2 (Fig. 1b, middle), but remains wet throughout phase 3. There are ensemble members in all phases that appear close to observed, and the observations were not unpredictable by all ensemble members.

We focus on the season closest to the observed driest or wettest season during each phase. This corresponds to FMA2006 (phase 1), ASO2006 (phase 2), and FMA2007 (phase 3). Figure 2 shows the area-averaged precipitation from all ensemble members verifying in the above seasons at short and long leads versus observed precipitation. The precipitation anomaly in millimeters per day is given on the *y* axis. On the *x* axis, we have binned ensemble members, that is, bin 1 houses the first ensemble member from each model (nine ensemble members, one from each model), bin 2 houses the second ensemble member from each model, and so on until bin 24, which houses the twenty-fourth ensemble member from each model (only one model has 24 ensemble members available). Note that the number of ensemble members per bin decreases with higher bin numbers because of the varying amount of ensemble members available in each model. We have masked out ensemble members showing neutral rainfall and thus only focus on rainfall in the upper and lower terciles. The number of ensemble members out of 109 falling into upper and lower categories is noted in the bottom right of each panel. The red dotted line indicates the value of the observed precipitation anomaly.

We find the best agreement during a short lead verifying in FMA2006 (Fig. 2, top left), with less agreement as lead time increases. The worst agreement occurs at a long lead verifying in FMA2007 (Fig. 2, bottom right), in which the NMME system shows predominantly wet anomalies in the Southeast region. We also find that the ensemble members that are able to capture below-normal rainfall during FMA2007 at a long lead do not capture the magnitude of the observed precipitation anomaly very well, with only a few exceptions. The majority of ensemble members show below-normal rainfall in ASO2006 at both lead times (Fig. 2, middle panels), though this period is only weakly above normal in observations, and its possible the NMME system is not capturing this accurately as the observed anomaly is small.

We have plotted the NMME ensemble mean anomaly (most probable outcome) for FMA2006, ASO2006, and FMA2007 at short and long leads versus observations in Figs. 3a, 3b, and 3c, respectively. Figure 3a (FMA2006) shows similar results to previous figures, with good

agreement at a short lead, and slightly dry, but mainly neutral, precipitation at a long seasonal lead. ASO2006 (Fig. 3b) accurately captures the precipitation deficit off the coast of the United States with a slight wet anomaly inland, but is mainly neutral at both leads. This season did not show good skill at either lead time, so this is expected. Finally, we find that the NMME system does not accurately resolve the precipitation anomalies in FMA2007 (Fig. 3c) at a long lead, showing a predominantly wet anomaly at this lead time and very weakly dry precipitation at a short seasonal lead.

Given this large tendency for above-normal precipitation during FMA2007 at a long lead, we also looked at the SSTA hindcast during this time period (Figs. 4a–c), as there is potential for a linkage to tropical Pacific SSTAs during the winter seasons. A more comprehensive analysis of SSTA skill in the NMME system is shown in Kirtman et al. (2014). Recall the results from Mo and Schemm (2008): cold (warm) ENSO brings dryness (wetness) in the Southeast in winter but brings wetness (dryness) in summer. In observations, we find cold SSTAs during phase 1, followed by warm SSTA in phase 2, and narrow, cold, more concentrated SSTAs in phase-3. We do not see a continual cold event in the tropical Pacific, and we find warm SSTAs in summer.

We find that during FMA2006, ASO2006, and FMA2007 (Figs. 4a–c) there is good agreement during the short-lead periods in the tropical Pacific, but during the long-lead hindcast, there are neutral SSTAs in FMA2006 and warm SSTAs in FMA2007; thus, the SSTA hindcast during these two time periods was incorrect. It is not apparent that the incorrect SSTA was causing the incorrect precipitation forecast or was in fact coincidental. Additional research must be carried out to understand the complete reasoning behind the incorrect hindcast, which can be due to, for example, resolution of phenomena (e.g., Stefanova et al. 2012), overall model skill or error, or parameterization of relevant physical processes, because prediction does not rely exclusively on these teleconnections.

b. Southeast US Rainfall Response to ENSO Diversity

Research has shown that there is significant diversity in the location of the maximum sea surface temperature anomaly (SSTA) associated with the El Niño Southern Oscillation (ENSO). In one extreme, the warm SSTA peak near the South American coast (often referred to as Eastern Pacific of EP El Niño), and at the other extreme, warm SSTA peak in the central Pacific (often referred to as Central Pacific or CP El Niño). Due to the differing tropical Pacific SSTA and precipitation structure, there are differing extratropical responses, particularly over North America. Recent work involving the North American Multi-Model Ensemble (NMME) System for Intra-Seasonal to Inter-Annual Prediction (ISI) on the accuracy of prediction of the differences between El Niño events found excess warming in the eastern Pacific during CP El Niño events. Infanti and Kirtman (2014b) follows from this analysis and investigates the certainty of the North American response to the diversity of ENSO, focusing on regional land-based 2-meter temperature and precipitation. Certainty in NMME predictions of North American precipitation and T2m is regional, and some regions, such as Southeast North America, demonstrate a strong connection to NINO3 precipitation and SSTA magnitude. Other regions, such as the Northwest North America, demonstrate a weak connection to NINO4 precipitation and SSTA magnitude. Still other regions do not show a strong connection between certainty and magnitude of tropical Pacific anomalies.

Here we show some specific examples of the analysis given in Infanti and Kirtman (2014b). For example, Figure 5a shows the probability density function (PDF) of NINO3 and NINO4 SSTA for all ensemble members and El Niño events, the x-axis is standardized. Ensemble members are binned based on standard deviation away from the mean, e.g. Bin 1 contains all ensemble members within 0 and 0.5 standard deviations from the mean (neutral SSTA), Bin 2

within 0.5 and 1 standard deviations from the mean, and so on. For all ensemble members in each bin, we find the corresponding North American regional precipitation, and plot resulting PDF (Fig. 5b-d). Dark blue (red) dashed contours highlight the precipitation PDF corresponding to neutral (strong positive) SSTA. Similar analysis, but binned according to tropical Pacific precipitation magnitude, is shown in Fig 6. In this case, red to blue PDFs correspond to weakest to strongest tropical Pacific precipitation. In terms of uncertainty, a centered, well-dispersed PDF would be uncertain, a PDF that is, for instance, shifted toward positive values, would show certainty in a positive response.

There is a clear linear relationship with NINO3 SSTA magnitude shown in Fig. 5b. The precipitation PDF corresponding to strong positive SSTA is almost entirely positive (thus more certain about positive precipitation), more centered is the PDF corresponding to neutral SSTA. Also more centered are SE precipitation PDFs corresponding to NINO4 SSTA (Fig. 5d), with the exception of the PDF corresponding to neutral SSTA showing a positive mean. Overall, however, precipitation corresponding to NINO4 SSTA does not show strong linearity.

Similar analysis for NW precipitation is shown in Fig. 5c,e. While there was some linearity between NINO4 SSTA magnitude and precent negative NW precipitation (Fig. 5b), this is not as apparent in this analysis. NW precipitation PDFs corresponding to NINO3 SSTA (Fig. 5c) are similar regardless of which Bin considered, the precipitation PDF corresponding to neutral (strong positive) SSTA shows a slight shift in the mean from negative to positive. NW PDF's corresponding to NINO4 SSTA (Fig. 5e) are also similar to each other, we only see a hint of linearity in the left tail of the distribution, where the PDF corresponding to neutral SSTA is slightly less negative that the PDF corresponding to the strong positive SSTA.

Figure 6a-e is similar, but binned based on NINO3 and NINO4 precipitation. Additional Bins (1-8) cover the full range of tropical Pacific precipitation (Fig 6a). The PDFs for SE precipitation corresponding to NINO3 and NINO4 precipitation are similar to the results for NINO3 and NINO4 SSTA. The linearity and shift of the PDFs toward positive values for stronger rainfall is more apparent when considering the PDFs corresponding to NINO3 precipitation (Fig. 6b). The PDFs corresponding to NINO4 precipitation show a shift toward positive values only in the mean of SE precipitation (Fig. 6d).

NW precipitation corresponding to NINO3 precipitation again shows little linearity (Fig. 6c). NW precipitation corresponding to NINO4 precipitation shows a slight shift towards negativity in the mean for strong positive NINO4 precipitation (Fig. 6e). Additionally, in the left and right tails of the distribution there is a shift toward more negative/less positive values as NINO4 precipitation magnitude increases, more apparent in the right tail. NINO4 precipitation explains significant variance of NW precipitation (Fig. 6b), however, for weak (strong) NINO4 precipitation approximately 42% (35%) of ensemble members predict above zero rainfall. Implicitly, this means that for weak (strong) NINO4 precipitation approximately 58% (65%) of ensemble members predicted below zero rainfall. While the slope is significant, these values are more neutral compared to, say, the SE, where for weak (strong) NINO3 precipitation approximately 45% (70%) of ensemble members predict above normal rainfall, and 55% (30%) below.

Figure 7a,b show NINO3 (Fig. 7a) and NINO4 (Fig. 7b) NMME SSTA magnitude vs. percent of ensemble members predicting positive and negative rainfall during each defined El Niño event in each North American region. NINO3 SSTA explains significant variance in the SW and SW, and NINO4 explains significant variance in the NW and NE. Slope of the linear regression line is significant for NINO3 SSTA versus the SE (Fig. 7a), and for NINO4 SSTA versus GP, NW, SW, and NW, though variance explained is not significant in the GP and SW. NINO3 also explains significant variance in the SW, but the slope is neutral, so it is likely that SSTA magnitude does not play a large role in precipitation agreement in this region. Overall,

precipitation agreement in the SW, NW, and NE show the strongest relationship with tropical Pacific SSTA magnitude.

The large explained variance and positive slope in the SE due to NINO3 SSTA indicates that as NINO3 SSTA magnitude increases, the agreement in predicting positive precipitation anomalies increases. The expected impact during EP events is positive precipitation in the southeast. In the NW, the larger NINO4 explained variance and negative slope is also optimistic, as the expected impact during CP events is negative in the region and the forecast agreement of negative precipitation anomalies increases. The northeast is negative during CP events and mixed positive and negative during EP though we find a stronger relationship with NINO4 SSTA.

For SSTA magnitude vs. T2m (Fig 7c,d) NINO3 SSTA explains significant variance in the SE, GP, and SW. NINO4 does not explain significant variance in any region. T2m is more closely related to anomalies in the NINO3 region, but the neutral slope in the GP, NW, and NE implies that magnitude does not exhibit a strong control on this variable. Magnitude is important in the SW and SE for T2m. The SW and SE are cold when there is NINO3 warming (negative slope).

We conduct similar analyses using NINO3 and NINO 4 NMME precipitation versus precent positive/negative ensemble members in Fig. 8a-b. Precipitation is perhaps a better proxy due to its control on atmospheric teleconnections. This analysis further refines the above conclusions. When considering North American precipitation, there is significant variance explained in the SE by NINO3 precipitation and in the NW and NE by NINO4 precipitation. The slope does not pass our significance test in any region, but are of the anticipated sign given the expected. Similarly, for North American T2m, we find that NINO3 precipitation explains significant variance in the SE, GP, SW, and NE, but the slope does not pass our significance test. We hesitate to state that there is no relationship between NINO3 and NINO4 magnitude and North American precipitation due to the lack of significance of the slope as there is still decidedly negative and positive slope shown for the given regions. The slope simply does not pass the current significance test. Lowering the significance level would change this conclusion.

c. Atmosphere-Land Coupling in the Interactive Ensemble

One of the proposed hypotheses for land-atmosphere interactions is due to stochastic forcing. In order to isolate the role of stochastic forcing we introduced the so-called interactive ensemble (Kirtman and Shukla 2002; Kirtman et al. 2003; Kirtman et al. 2005; Kirtman et al. 2009; Kirtman et al. 2011; Lopez and Kirtman 2014). The interactive ensemble implementation developed for the NCAR family of models (CCSM3, CCSM4 and CESM1) uses multiple realizations of the atmospheric model (CAM) coupled to a single realization of the ocean model (POP), a single realization of the sea-ice model and a single realization of the land-surface model. The coupling of the multiple realizations of CAM to the single realizations of the other component models is accomplished through the CCSM coupler. The purpose of this coupling strategy is to significantly reduce the stochastic forcing of the ocean due to internal atmospheric dynamics. Ensemble averaging of fluxes of heat, momentum and fresh water produced by the individual CAM ensemble members before they are passed to POP effectively filters the noise in the fluxes due to internal atmospheric dynamics. Additional details can be found in Kirtman et al. (2009).

Over the ocean this approach works well since the coupling is entirely through the fluxes and the ensemble averaging of the fluxes is found to due little damage to the mean state of the coupled system (see Kirtman et al. 2009, 2011). However, over the ice and land the coupling includes fluxes and state variables that are used by the component models to calculate fluxes. The ensemble averaging, therefore, has a disproportionately large effect on state variables

compared to flux fields, which ultimately leads to differences in the climatology of ice and land that are too large. For instance, over ice and land wind-dependent fluxes are calculated using the ensemble mean *state* (as opposed to flux) variables leading to strong biases over land and ice. We refer to this particular implementation of the interactive ensemble as "IE(mean coupling)" to emphasize that over land and ice the turbulent fluxes compared to the radiative fluxes are disproportionately affected by the ensemble averaging (see Fig. 9a).

Our first approach to alleviate the problem was to focus on the atmosphere-land and atmosphere-ice coupling. In a second implementation of the interactive ensemble we isolated a single atmosphere for the atmosphere-land and atmosphere-ice coupling. Essentially, the root or the single atmosphere is fully coupled to the land and ice and the remaining atmospheres experience the land and ice state, but do not modify the land and ice properties through their fluxes. The other atmospheres are effectively de-coupled at the atmosphere-land and atmosphere-ice interface. This implementation of the interactive ensemble is referred to as "IE(one land)" to emphasize that over land and ice all coupling is via a single atmosphere (Fig. 9b).

Figure 9a shows the surface temperature bias (control minus interactive ensemble) for a 250-year simulation using IE(mean coupling) and 9b shows the surface temperature bias for a 250-year simulation using IE(one land). Clearly, the surface temperature bias is reduced with IE(one land), and in fact, we assert that the large surface temperature differences over the terrestrial northern Hemisphere are associated with a colapse of the Atlantic Meridional Overturing Circulation (AMOC) which could not be isolated with IE(mean coupling).

While IE(one land) clearly reduces the surface temperature bias, the de-coupled atmospheres are energetically inconsistence at the atmosphere-land and atmsophere-ice interface. This energetic inconsitency has the potential to significantly affect the variability (see Fig. 9a) in much the same way the prescribed SSTs artifically enhance simulated atmospheric variability over the ocean (e.g., Wu and Kirtman 2007). To remove the energetic inconsistency at the atmosphere-land and atmosphere-ice interface, we implemented a third version of the interactive ensemble where each atmospheric realization is coupled to its own land and own ice component models. We refer to this interactive ensemble implmentation at IE(multi-land) to emphasize that each atmospheric component is coupled to its own land and ice component models. This third implementation removes the bias issue noted in Fig. 9 and removes the variability problem seen in Fig. 10a (see results in 10b). The large differnces in variability seen over South America can be confidently ascribed to the reduced SST variability in the IE simulations. These results are being prepared for publication.

3. Highlights of Accomplishments

- Completion of the first set of numerical experiments.

- Diagnosis of how atmospheric noise impacts the externally forced rainfall response over North America.

- Showed how land surface and atmospheric initialization impacts seasonal predictability and prediction skill

- Examined the hindcast skill on the 2006-2007 Southeast US drought.

- Developed new interactive ensemble coupling approaches to isolate land-atmosphere interactions

4. Publications from the Project

Achuthavarier, D., V. Krishnamurthy, B. P. Kirtman and B. Huang, 2012: Role of Indian Ocean in the ENSO-Indian summer monsoon teleconnection in the NCEP climate forecast system. J. Climate, doi: http://dx.doi.org/10.1175/JCLI-D-11-00111.1.

Chen, H., E. K. Schneider, B. P. Kirtman, I. Colfescu, 2013: Evaluation of weather noise and its role in climate model simulations. J. Climate, doi:10.1175/JCLI-D-12-00202.

DiNezio, P. N., B. P. Kirtman, A. C. Clement, S.-K. Lee, G. A. Vecchi, A. Wittenberg, 2012: Diverging ENSO projection in response to global warming: The role of the background ocean changes. *J. Climate* doi: http://dx.doi.org/10.1175/JCLI-D-11-00494.1.

Goddard, L, A. Kumar, A. Solomon, D. Smith, G. Boer, P. Gonzalez, C. Deser, S. Mason, B. Kirtman, R. Msadek, R. Sutton, E. Hawkins, T. Fricker, S. Kharin, W. Merryfield, G. Hegerl, C. Ferro, D. Stephenson, G.A. Meehl, T. Stockdale, R. Burgman, A. Greene, Y. Kushnir, M. Newman, J. Carton, I. Fukumori, D. Vimont, T. Delworth, 2013: A verification framework for interannual to decadal prediction experiments, *Climate Dynamics* 40, 245-272.

Goddard, L., J. W. Hurrell, B. P. Kirtman, J. Murphy, T. Stockdale and C. Vera, 2012: Two timescales for the price of one (almost). *Bull. Amer. Met. Soc.*, doi: http://dx.doi.org/10.1175/BAMS-D-11-00220.1

Infanti, J. M., and B. P. Kirtman, 2014a: Southeast US Rainfall Prediction in the North American Multi-Model Ensemble. *J. Hydrometeor*, 15, 529-550.

Infanti, J. M., and B. P. Kirtman, 2014b: Uncertainty of the North American rainfall and temperature response to the diversity of ENSO in the North American Multi-Model Ensemble. J. Climate (submitted).

Kirtman, B. P., E. K. Schneider, D. M. Straus, D. Min, R. Burgman, 2011: How weather impacts the forced climate response. *Climate Dynamics*, DOI : 10.1007/s00382-011-1084-3.

Kirtman, B. P., and co-authors, 2012: Impact of ocean model resolution on CCSM climate simulations. *Climate Dynamics,* DOI 10.1007/s00382-012-1500-3.

Kirtman, B. P., T. Stockdale and R. Burgman, 2013: The Oceans' role in modeling and predicting seasonal-to-interannual climate variations. Ocean Circulation and Climate: A 21st Century Perspective (2nd Edition). G. Siedler, S. Griffies, J. Gould and J. Church, Eds. Academic Press (Elsevier) DOI 10.1016/B978-0-12-391851-2.00024-6.

Kirtman, B. P., D. Anderson, G. Brunet, I.-S. Kang, A. A. Scaife and D. Smith, 2013: Prediction from weeks to decades, *Climate Science for Serving Society: Research, Modelling and Prediction Priorities*. G. R. Asrar and J. W. Hurrell, Eds. Springer, DOI 10.1007/978-94-007-6692-1_8.

Kirtman, B. P., and co-authors, 2014: The North American Multi-Model Ensemble (NMME): Phase-1 Seasonal-to-Interannual Prediction, Phase-2 Toward Developing Intra-Seasonal prediction. Bull. Amer. Met. Soc., doi: 10.1175/BAMS-D-12-00050.1.

Larson, S., and B. P. Kirtman, 2013: The Pacific meridional mode as a trigger for ENSO in a high-resolution coupled model. Geophys. Res. Lett., DOI: 10.1002/grl.50571.

Lee, S.-K., W. Park, E. van Sebille, M. O. Baringer, C. Wang, D. B. Enfield, S. G. Yeager, and B. P. Kirtman (2011), What caused the significant increase in Atlantic Ocean heat content since the mid-20th century?, Geophys. Res. Lett., 38, L17607, doi:10.1029/2011GL048856.

Lopez, H., B. P. Kirtman et al., 2013: Impact of interactive westerly wind bursts on CCSM3. Dyn. Atmos. Ocean, **59**, 24-39.

Munoz, E., B. Kirtman, and W. Weijer, 2011: Varied representation of the Atlantic Meridional Overturning across multidecadal ocean reanalyses. *Deep Sea Research Part II*, doi:10.1016/j.dsr2.2010.10.064.

Narapusetty, B., C. Stan, B. P. Kirtman, P. S. Schopf, L. Marx, and J. L. Kinter III (2012), The role of atmospheric internal variability on the tropical instability wave dynamics, J. Geophys. Res., 117, C00J31, doi:10.1029/2012JC007906.

Narapusetty, B., and B. Kirtman, 2014: Sensitivity of near-surface atmospheric circulation to tropical instability waves. *Climate Dynamics*, 10.1007/s00382-014-2167-8.

Paolino, Daniel A., James L. Kinter, Ben P. Kirtman, Dughong Min, David M. Straus, 2012: The Impact of Land Surface and Atmospheric Initialization on Seasonal Forecasts with CCSM. *J. Climate*, **25**, 1007–1021; doi: http://dx.doi.org/10.1175/2011JCLI3934.1.

Siqueira, L. S. P., and B. P. Kirtman, 2012: Predictability and uncertainty in a low order coupled model. *Nonlinear Process in Geophysics* doi:10.5194/npg-19-273-2012.

Siqueira, L. and Kirtman, B. 2014: Nonlinear dynamics approach to the predictability of the Cane–Zebiak coupled ocean–atmosphere model, *Nonlin. Processes Geophys.,* 21, 155-163, doi:10.5194/npg-21-155-2014, 2014.

Smith, D. M., A. A. Scaife and B. P. Kirtman, 2012: What is the current state of scientific knowledge with regard to seasonal and decadal forecasting? Environ. Res. Lett., 015602 doi:10.1088/1748-9326/7/1/015602.

Smith, D. M., A. A. Scaife and B. Kirtman, 2012: What is the current state of scientific knowledge with regard to seasonal and decadal forecasting. Environ. Res. Lett., 7 015602, doi:10.1088/1748-9326/7/1/015602.

Smith, D. M., (B. P. Kirtman) et al., 2013: Real-time multi-model decadal climate predictions. *Clim. Dyn.,* doi:10.1007/s00382-012- 1600-0.

Solomon, Amy, and Coauthors (… B. P. Kirtman …), 2011: Distinguishing the Roles of Natural and Anthropogenically Forced Decadal Climate Variability. Bull. Amer. Meteor. Soc., 92, 141–156. doi: 10.1175/2010BAMS2962.1

Yeh, S.-W., B. P. Kirtman, J.-S. Kug, W. Park, and M. Latif (2011), Natural variability of the central Pacific El Niño event on multi-centennial timescales, *Geophys. Res. Lett.*, 38, L02704, doi:10.1029/2010GL045886.

Yeh, S. –W., Y. –G. Ham, B. P. Kirtman, 2014: A possible explanation on the changes in the spatial structure of ENSO from CMIP3 to CMIP5. *Geophys. Res. Lett.*, doi: 10.1002/2013GL058478.

5. PI contact information

Benjamin P. Kirtman

Rosentiel School of Marine and Atmospheric Science

University of Miami

4600 Rickenbacker Causeway

Miami, FL 33149

E-mail: bkirtman@rsmas.miami.edu

Phone: (305)412-4046

Tables and Figures

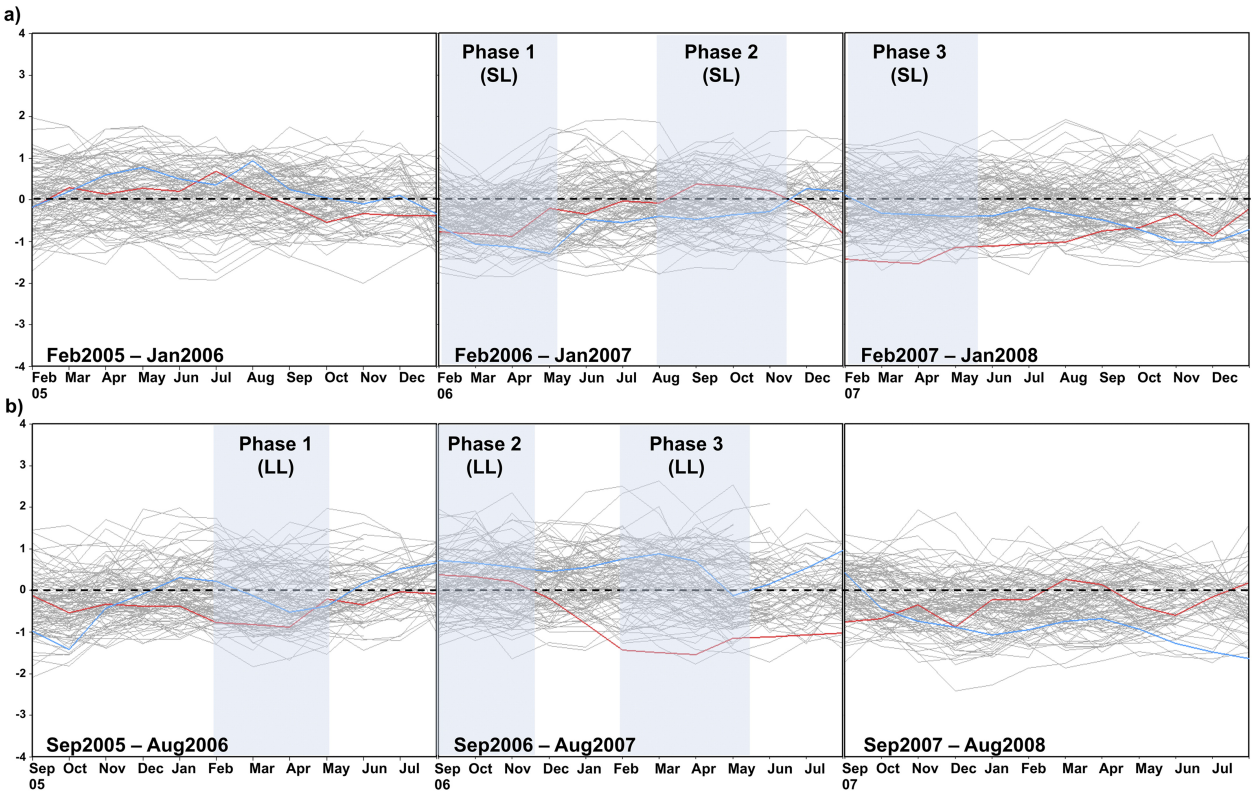

Figure 1: NMME hindcast plumes for the period between February 2005 thru August 2008 for hindcasts initialized in (a) February and (b) September 2005. Hindcast is initialized at the beginning of each panel with lead time increasing along the *x* axis. Red lines show observed standardized (divided by standard deviation) precipitation anomaly, blue lines show standardized NMME ensemble mean precipitation anomaly, and gray lines indicate standardized individual ensemble member precipitation anomalies. Units are mm day^{-1} per standard deviation. Vertical shading represents phases 1, 2, and 3 of the 2006–07 southeastern U.S. drought.

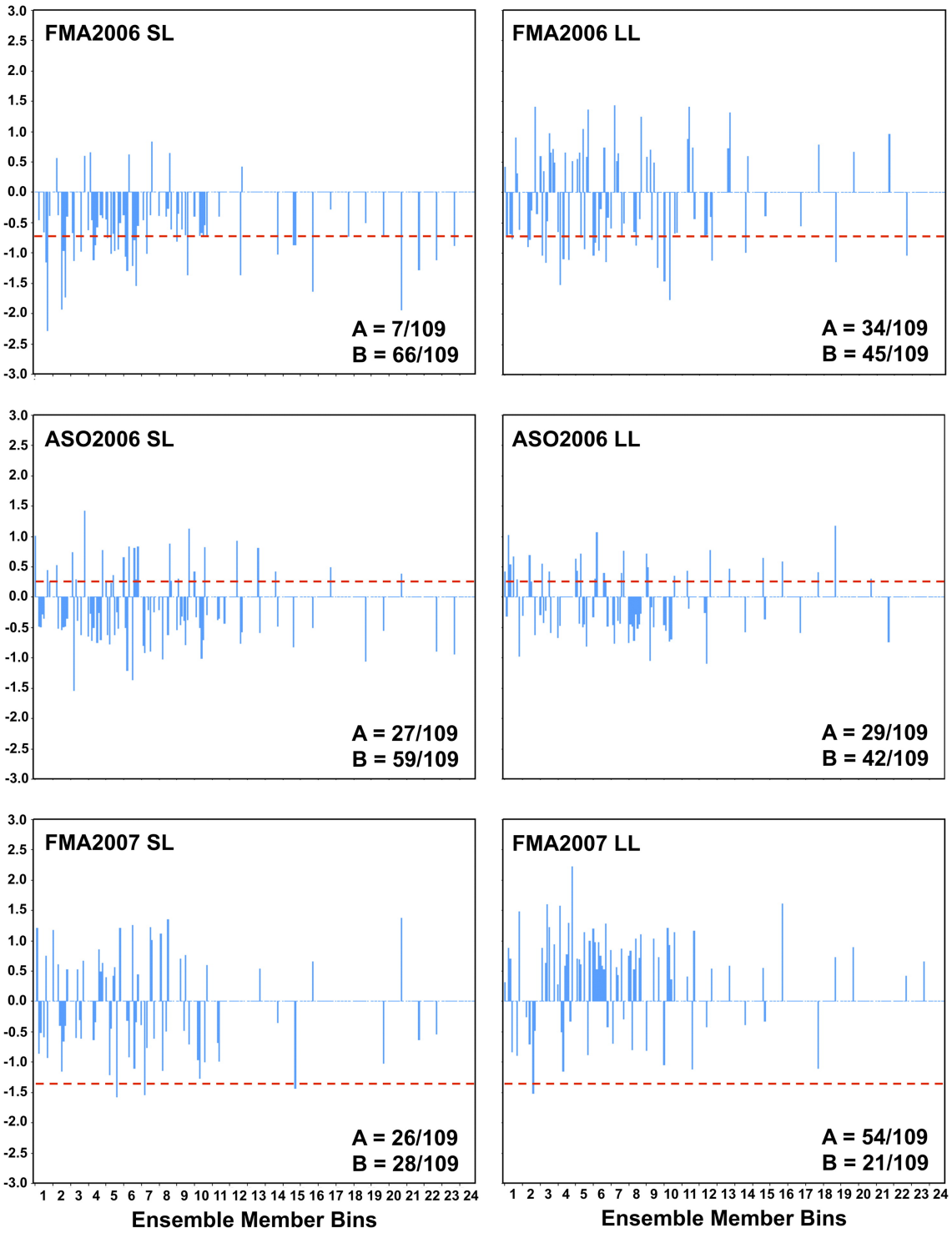

Figure 2: Area-averaged ensemble members vs area-averaged observed precipitation anomaly grouped by ensemble member. Only ensemble members with above- and below-normal rainfall are plotted; neutral ensemble members are masked out. Blue bars indicate precipitation anomaly for each ensemble member, binned according to ensemble member. Bin 1 is the first ensemble member from each model, bin 2 is the second ensemble member, and so on to bin 24, the twenty-fourth ensemble member from each model (only one model has 24 ensemble

members available). Horizontal red dashed lines indicate the approximate observed precipitation anomaly. Units are mm day^{-1}ranging from −3.0 to 3.0 on the *y* axis. The designation letters A and B indicate the number of ensemble members predicting above- or below-normal rainfall. For example, for FMA2006 at a short lead time, A = 7/109 indicates that 7/109 ensemble members predict above-normal rainfall, and B = 66/109 that 66/109 ensemble members predict below-normal rainfall.

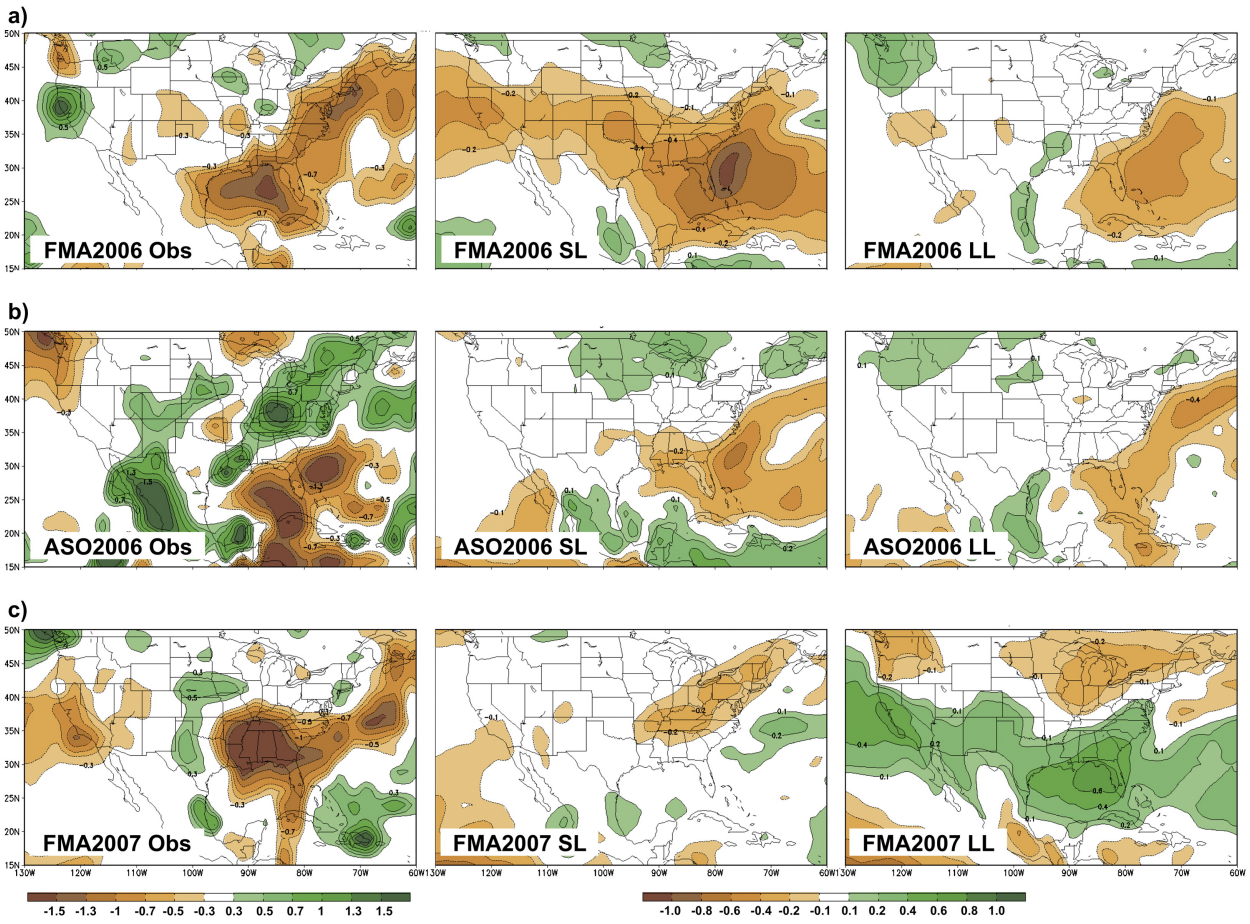

Figure 3: (left) Observed vs NMME ensemble mean precipitation anomalies for (middle) short and (right) long leads for (a) FMA2006, (b) ASO2006, and (c) FMA2007. Observed is plotted for phase 1 through phase 3 of the 2006–07 drought and has a color scale and contours ranging from −1.5 to 1.5 mm day^{-1} at intervals of 0.3, 0.5, 0.7, 1.0, 1.3, and 1.5 mm day^{-1}. NMME ensemble mean verifies in the same seasons at the short and long leads and has a color scale and contours ranging from −1 to 1 mm day^{-1} at intervals of 0.1, 0.2, 0.4, 0.6, 0.8, and 1.0 mm day^{-1}. The *y*axes run from 15° to 50°N in increments of 5° and the *x* axes run from 130°W to 60°W in increments of 10°.

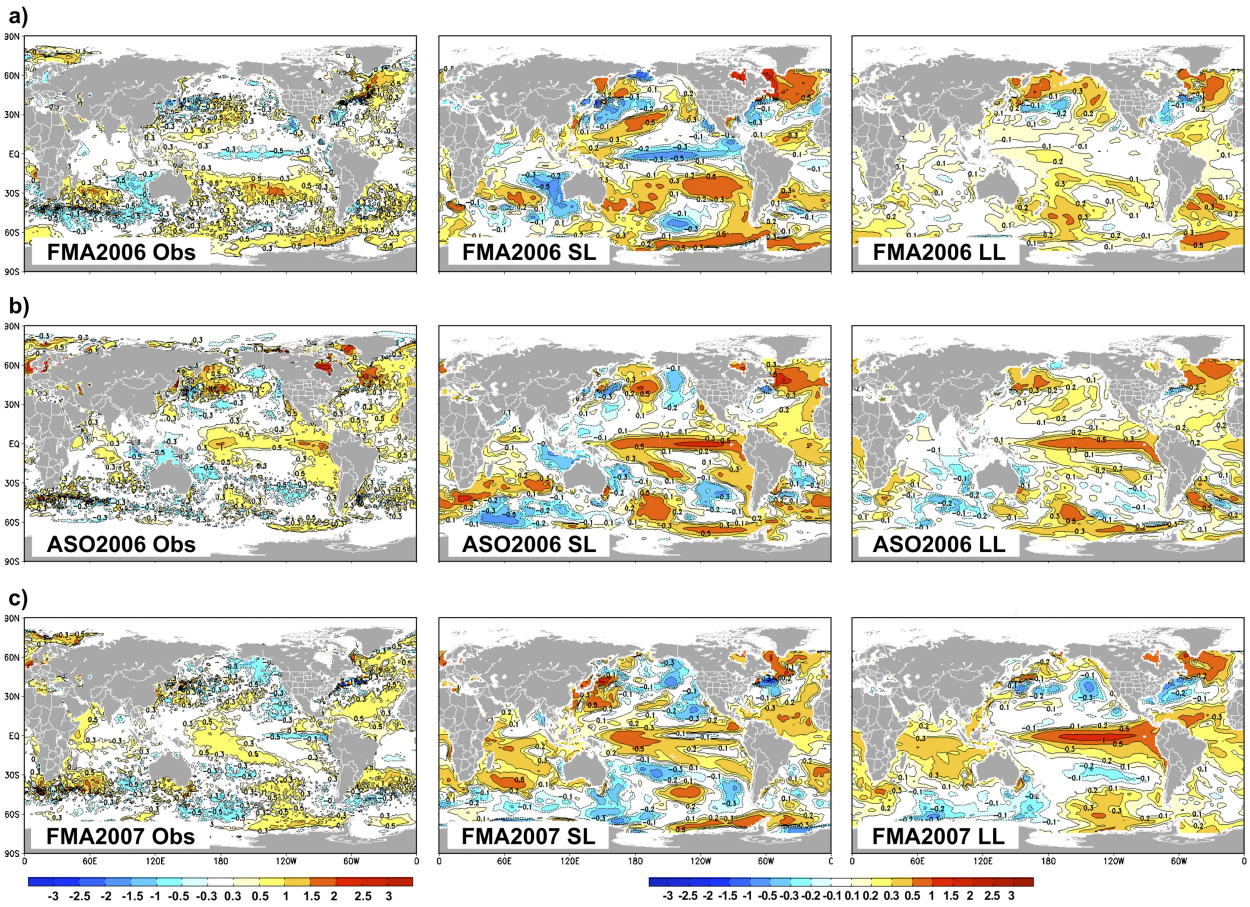

Figure 4: As in Fig. 3, but for SSTA.

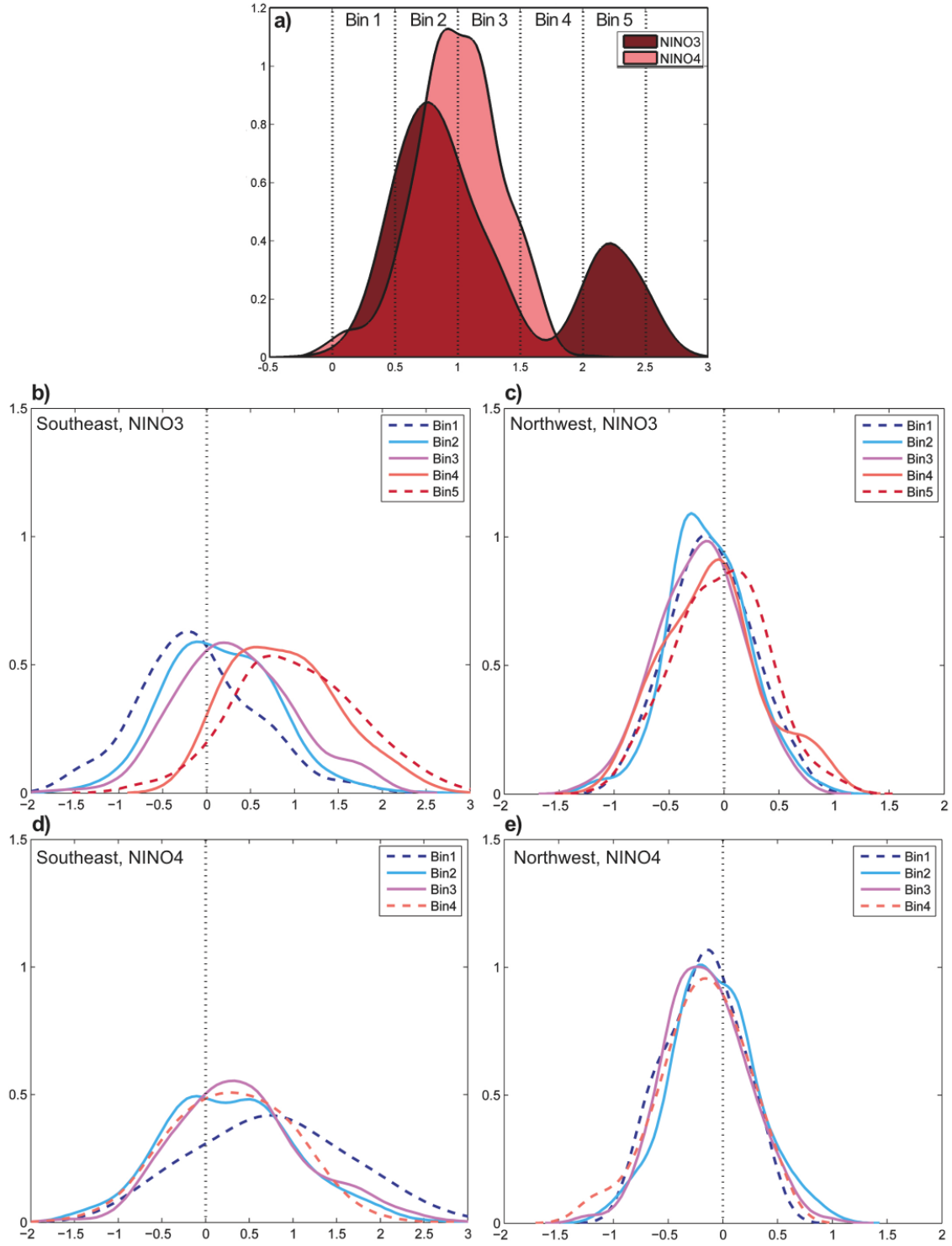

Figure 5: a) Probability density function of NMME NINO3 and NINO4 SSTA during defined EP and CP El Nino events. Y-Axis shows probability density. X-axis shows standardized SSTA. Bin 1 through Bin 5 refers to the ensemble members with NINO3 or NINO4 SSTA falling into neutral (0 to 0.5σ) to strongly positive (2 to 2.5σ) categories. The amount of ensemble members included in Bin 1 for NINO3 SSTA is 97, Bin 2 is 386, Bin 3 is 162, Bin 4 is 30, and Bin 5 is 165. The amount of ensemble members included in Bin 1 for NINO4 SSTA is 59, Bin 2

is 372, Bin 3 is 369, Bin 4 is 67, and Bin 5 is 1. Note that due to the low amount of ensemble members in Bin 5 NINO4 SSTA, we do not include this Bin in the remaining analysis. b) Probability density function for southeast Precipitation corresponding to NINO3 SSTA. The PDF for Bin 1 includes the ensemble member precipitation corresponding to neutral (0 to 0.5σ) NINO3 SSTA. The PDF for Bin 5 includes the ensemble member precipitation corresponding to strongly positive (2 to 2.5σ) NINO3 SSTA. Dark blue to red color scale indicates PDFs corresponding to neutral to strongly positive SSTA. Dashed contours indicate PDF corresponding to neutral or weakest SSTA (blue) and strongest SSTA (red). c) As in (a), but for Northwest precipitation. d) As in (a), but corresponding to NINO4 SSTA. e) As in (c), but corresponding to NINO4 SSTA.

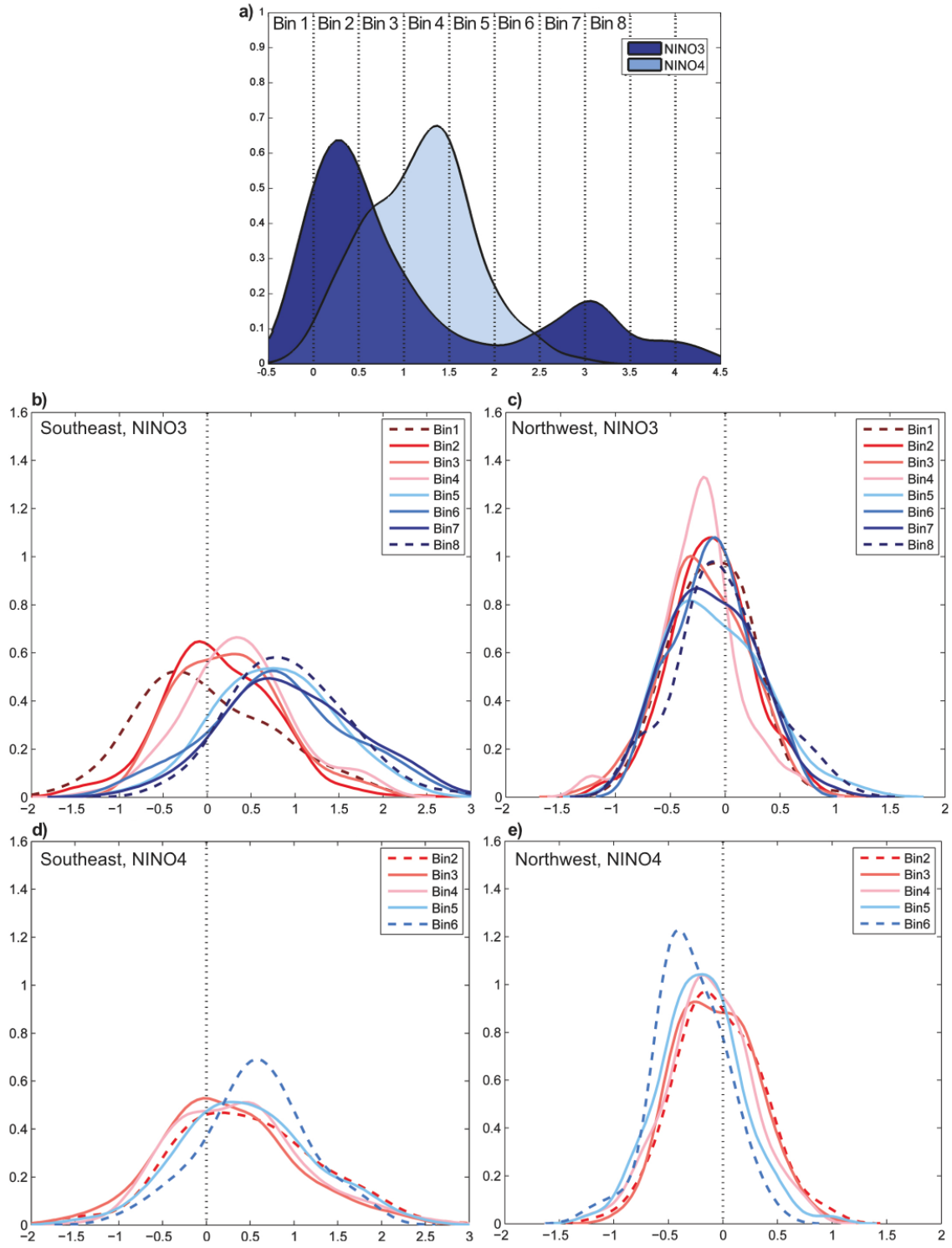

Figure 6: As in Fig. 5, but corresponding to NINO3 and NINO4 precipitation. The amount of ensemble members in each NINO3 bin are as follows: 109, 291, 165, 72, 25, 28, 61, and 68. The amount of ensemble members in each NINO4 bin are as follows: 12, 112, 201, 292, 183, 58, 13, 1. Note that due to the low amount of ensemble members in NINO4 Bins 1, 7 and 8, they are not included in the remaining analysis. Red dashed contours indicates PDF

corresponding to neutral or weak NINO3 or NINO4 precipitation, blue dashed contour indicates PDF corresponding to strongly positive NINO3 or NINO4 precipitation.

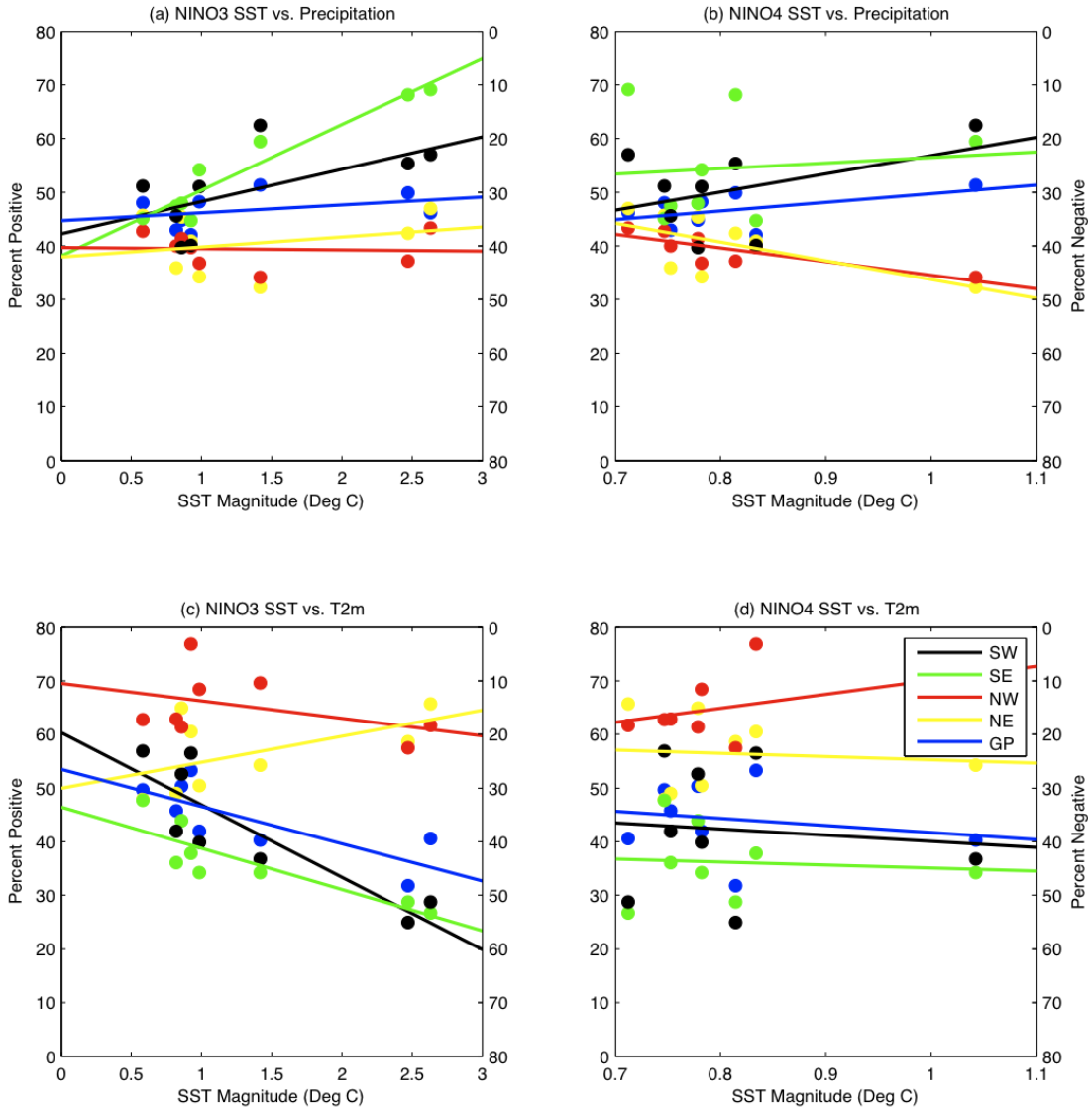

Fig. 7: Percent of ensemble members agreeing on the sign of the anomaly for each North American region. Left axis shows percent of ensemble members agreeing on above zero anomalies, right axis shows percent of ensemble members agreeing on below zero anomalies. X-axis shows NMME ensemble mean SST magnitude in degrees C. a) NMME NINO3 SSTA magnitude vs. North American regional precipitation percent correct. b) As in (a), but for NINO4 SSTA magnitude. c) NMME NINO3 SSTA magnitude vs. North American regional T2m amount correct. d) As in (c), but for NINO4 SSTA magnitude.

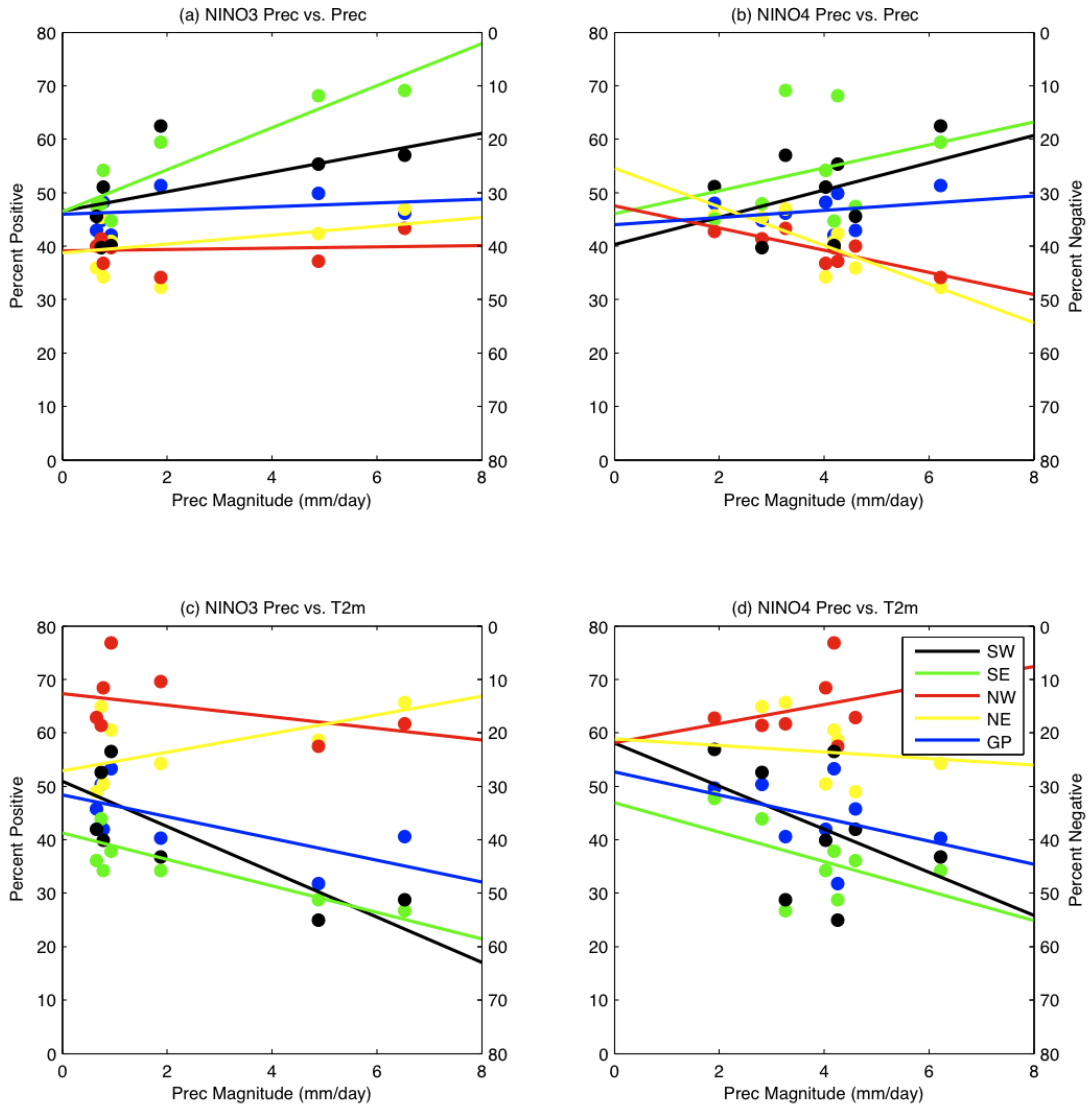

Fig. 8: As in Fig. 7, but plotted against NMME NINO3 and NINO4 precipitation magnitude.

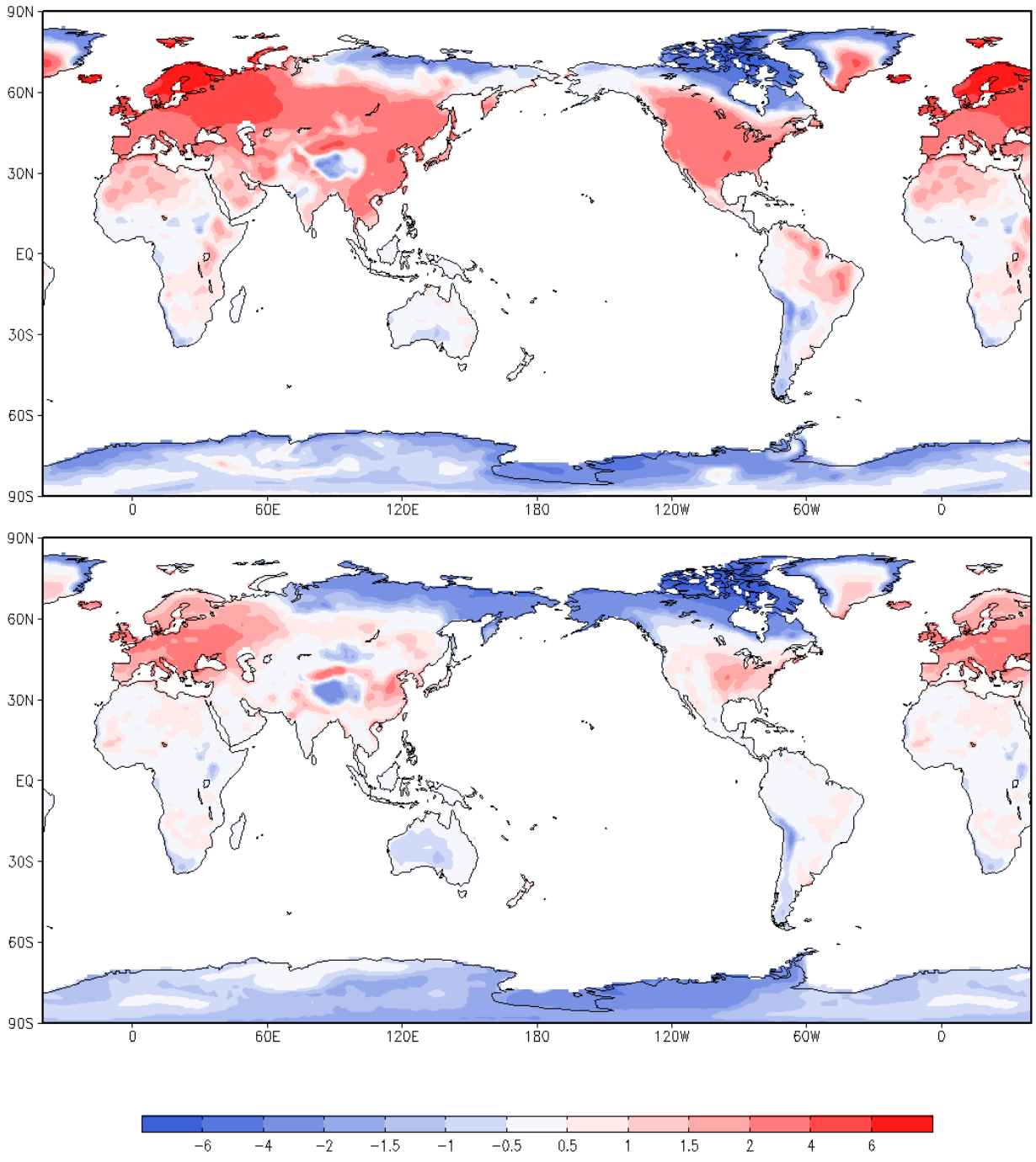

Figure 9: (a) CCSM4 annual mean surface temperature difference control minus interactive ensemble [IE(mean coupling)] for a 250-year simulations. (b) CCSM4 annual mean surface temperature difference control minus IE(one land).

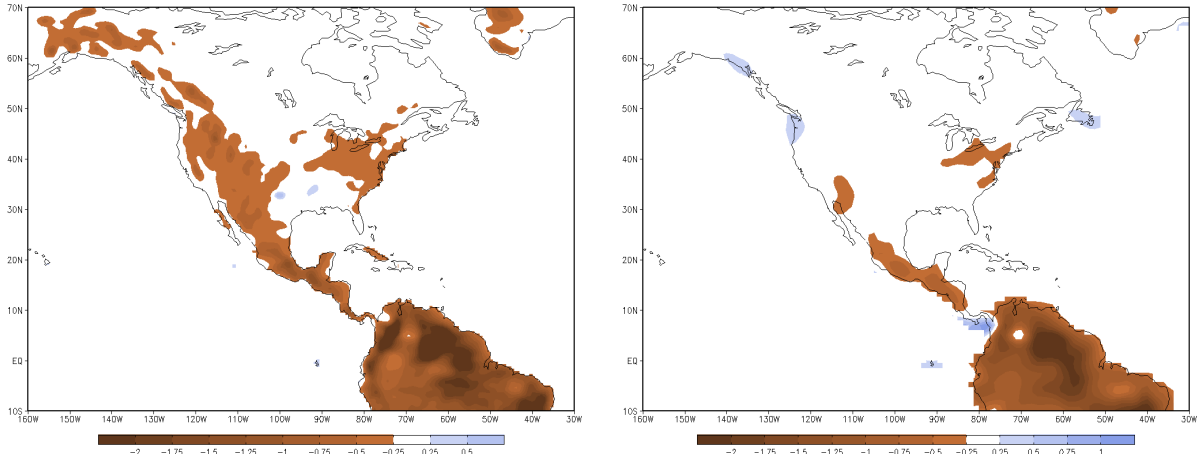

Figure 10: Difference in precipitation (mm per day) standard deviations for control minus IE (mean coupling) in the left panel and for control minus IE (multi land) in the right panel.